Oxide-Dependent Adsorption of a Model Membrane Phospholipid, Dipalmitoylphosphatidylcholine: Bulk Adsorption Isotherms

Timothy A. Oleson*,† and Nita Sahai†,‡,§

Department of Geology & Geophysics, 1215 West Dayton Street, University of Wisconsin, Madison, Wisconsin 53706, and Department of Chemistry, 1101 University Avenue, University of Wisconsin, Madison, Wisconsin 53706

Received November 18, 2007. In Final Form: January 8, 2008

The importance of substrate chemistry and structure on supported phospholipid bilayer design and functionality is only recently being recognized. Our goal is to investigate systematically the substrate-dependence of phospholipid adsorption with an emphasis on oxide surface chemistry and to determine the dominant controlling forces. We obtained bulk adsorption isotherms at 55 °C for dipalmitoylphosphatidylcholine (DPPC) at pH values of 5.0, 7.2, and 9.0 and at two ionic strengths with and without Ca^{2+}, on quartz (α-SiO_2), rutile (α-TiO_2), and corundum (α-Al_2O_3), which represent a wide a range of points of zero charge (PZC). Adsorption was strongly oxide- and pH-dependent. At pH 5.0, adsorption increased as quartz < rutile ≈ corundum, while at pH 7.2 and 9.0, the trend was quartz ≈ rutile < corundum. Adsorption decreased with increasing pH (increasing negative surface charge), although adsorption occurred even at pH ≥ PZC of the oxides. These trends indicate that adsorption is controlled by attractive van der Waals forces and further modified by electrostatic interactions of oxide surface sites with the negatively charged phosphate ester ($-R(PO_4^-)R'-$) portion of the DPPC headgroup. Also, the maximum observed adsorption on negatively charged oxide surfaces corresponded to roughly two bilayers, whereas significantly higher adsorption of up to four bilayers occurred on positively charged surfaces. Calcium ions promote adsorption beyond a second bilayer, regardless of the sign of oxide surface charge. We develop a conceptual model for the structure of the electric double layer to explain these observations.

1. Introduction

Supported phospholipid bilayers (SPBs) have been extensively studied in the context of biological and biomedical devices. Early work utilized SPBs as stationary cell membrane mimics for use in cell−cell recognition and membrane dynamics studies.[1,2] Efforts to understand membrane-related cellular processes[3,4] and biomolecular characteristics such as in situ protein structures[5−8] continue to be of great interest. The tremendous potential to exploit SPBs in novel biotechnological devices such as biosensors and mimetic membrane-coated implants has been recognized.[9−11] In both applications, a phospholipid (PL) bilayer adhered to a solid (often oxide) support is used to anchor biofunctional molecules. Myriad uses for biosensors have been proposed including, but not limited to, specific molecular (e.g., DNA, drugs) detection for medical diagnostics, cell typing, and inclusion in electronic circuits.[3,9−13] In the case of implant devices, it is proposed that supported bilayers or supported, tethered monolayers can be specifically impregnated with lipopeptides, whole proteins, and other molecules in order to increase biocompatibility, reduce the risk of host body rejection, and even promote new tissue growth.[10,14−16] Supported phospholipid bilayers have also been suggested for drug and bactericide delivery mechanisms,[17,18] prevention of biofouling,[6] control of pyrite toxicity in the environment,[19] and in templating controlled nanoparticle growth.[20−22] More generally, mineral surface−amphiphile (e.g., lipids or lipid precursors) interactions have been postulated to play an important role in the early evolution of life during the cellularization and compartmentalization steps.[23,24]

Numerous efforts have been made to characterize the formation and structure of SPBs following adsorption of free vesicles from

* Corresponding author. Telephone: (608) 262-4972. Fax: (608) 262-0693. E-mail: toleson@geology.wisc.edu.
† Department of Geology & Geophysics.
‡ Department of Chemistry.
§ E-mail: sahai@geology.wisc.edu.

(1) Margolis, L. B. *Biochim. Biophys. Acta* **1984**, *779*, 161−189.
(2) McConnell, H. M.; Watts, T. H.; Weis, R. M.; Brian, A. A. *Biochim. Biophys. Acta* **1986**, *864*, 95−106.
(3) Sackmann, E. *Science* **1996**, *271*, 43−48.
(4) Burgess, J. D.; Rhoten, M. C.; Hawkridge, F. H. *J. Am. Chem. Soc.* **1998**, *120*, 4488−4491.
(5) Reviakine, I.; Bergsma-Schutter, W.; Brisson, A. *J. Struct. Biol.* **1998**, *121*, 356−362.
(6) Glasmästar, K.; Larsson, C.; Höök, F.; Kasemo, B. *J. Colloid Interface Sci.* **2002**, *246*, 40−47.
(7) Salafsky, J.; Groves, J. T.; Boxer, S. G. *Biochemistry* **1996**, *35*, 14773−14781.
(8) Mueller, H.; Butt, H.-J.; Bamberg, E. *J. Phys. Chem. B* **2000**, *104*, 4552−4559.
(9) Krysiñki, P.; Tien, H. T.; Ottova, A. *Biotechnol. Prog.* **1999**, *15*, 974−990.
(10) Kasemo, B. *Surf. Sci.* **2002**, *500*, 656−677.
(11) Castellana, E. T.; Cremer, P. S. *Surf. Sci. Rep.* **2006**, *61*, 429−444.
(12) Cornell, B. A.; Braach-Maksvytis, V. L. B.; King, L. G.; Osman, P. D. J.; Raguse, B.; Wieczorek, L.; Pace, R. J. *Nature* **1997**, *387*, 580−583.
(13) Buranda, T.; Huang, J.; Ramarao, G. V.; Ista, L. K.; Larson, R. S.; Ward, T. L.; Sklar, L. A.; Lopez, G. P. *Langmuir* **2003**, *19*, 1654−1663.
(14) Tirrell, M.; Kokkoli, E.; Biesalski, M. *Surf. Sci.* **2002**, *500*, 61−83.
(15) Collier, J. H.; Messersmith, P. B. *Annu. Rev. Mater. Res.* **2001**, *31*, 237−263.
(16) Winger, T. M.; Ludovice, P. J.; Chaikof, E. L. *Langmuir* **1999**, *15*, 3866−3874.
(17) Moghimi, S. M.; Hunter, A. C.; Murray, J. C. *FASEB J.* **2005**, *19*, 311−330.
(18) Bennett, T. C.; Creeth, J. E.; Jones, M. N. *J. Liposome Res.* **2000**, *10*, 303−320.
(19) Zhang, X.; Borda, M. J.; Schoonen, M. A. A.; Strongin, D. R. *Langmuir* **2003**, *19*, 8787−8792.
(20) Bégu, S.; Girod, S.; Lerner, D. A.; Jardiller, N.; Tourné-Péteilh, C.; Devoisselle, J.-M. *J. Mater. Chem.* **2004**, *14*, 1316−1320.
(21) El Rassy, H.; Belamie, E.; Livage, J.; Coradin, T. *Langmuir* **2005**, *21*, 8584−8587.
(22) Baca, H. K.; Ashley, C.; Carnes, E.; Lopez, D.; Flemming, J.; Dunphy, D.; Singh, S.; Chen, Z.; Liu, N. G.; Fan, H. Y.; López, G. P.; Brozik, S. M.; Werner-Washburne, M.; Brinker, C. J. *Science* **2006**, *313*, 337−341.
(23) Trevors, J. T. *Antonie Van Leeuwenhoek* **1997**, *71*, 363−368.
(24) Hanczyc, M. M.; Fujikawa, S. M.; Szostak, J. W. *Science* **2003**, *302*, 618−622.

10.1021/la703599g CCC: $40.75
Published on Web 03/19/2008

solution[25−32] using experimental techniques such as force microscopy,[27,33−41] quartz crystal microbalance (QCM-D),[25−28,38,40,42−44] ellipsometry,[27,45] fluorescence techniques,[41,42,46−48] and neutron reflectivity,[29,49,50] as well as modeling and simulation methods.[30,51−53] Results have elucidated a three-step mechanism whereby vesicles adsorb, fuse, and eventually rupture to form planar bilayers. Specific contributing factors include vesicle size[25,54] and composition,[38,40,42,55,56] solution pH and ionic strength,[26,47,56−60] and temperature.[25,26,51,61,62] Structural, thermotropic, and dynamic characteristics of lipids in SPBs have also been well-characterized.[63−70]

The role of the substrate surface in vesicle adhesion and SPB formation has been studied in a relatively small group of materials, primarily, gold, mica, glass, silica, and quartz. Surface chemistry and charge,[25,26,47,58,63,71−79] hydrophilicity versus hydrophobicity,[30,71,80] and surface topography have been suggested as contributing factors.[25,45,47] A few groups have recently broadened the scope of supports studied to include TiO_2[18,25,42,54,72,81−84] and Al_2O_3[46,81,85] and have considered the role of surface charge identified by the point of zero charge (PZC) of the oxides.[25]

In this study, we determined bulk adsorption isotherms at 55 °C for pure dipalmitoylphosphatidylcholine (DPPC) vesicles at three pH values (5.0, 7.2, and 9.0) and two different ionic strengths on quartz (α-SiO_2), rutile (α-TiO_2), and corundum (α-Al_2O_3) particles, with the goal of elucidating oxide-dependent effects related to oxide surface charge. Phosphatidylcholine is a common membrane phospholipid, and oxides have relatively simple chemistry and stability over a wide pH range. Quartz, rutile, and corundum were chosen specifically because of their biomedical relevance and because their PZCs span a wide pH range, allowing for a systematic and quantitative investigation of DPPC adsorption and the dominant forces involved.

2. Experimental Section

2.1. Materials. We used zwitterionic 1,2-dipalmitoyl-*sn*-glycero-3-phosphocholine (DPPC, $C_{40}H_{80}NO_8P$, 99% purity, Avanti Polar Lipids Inc., Alabaster, AL), and *N*-(2-hydroxyethyl)piperazine-*N*′-2-ethanesulfonic acid (HEPES) buffer (molecular biology grade, Fisher Scientific, Inc., Waltham, MA). HEPES was chosen because it has smaller effects on the kinetics and adsorption of phosphatidylcholine (PC) on SiO_2 than Tris buffer [i.e., tris(hydroxymethyl)-aminomethane].[26,57] Also, HEPES does not interfere with the quantitative inorganic phosphorus analysis technique for [DPPC] determination used here. All other reagents (ACS grade) were purchased from either Fisher or Sigma-Aldrich (St. Louis, MO). Corundum (α-Al_2O_3, identified as Al_2O_3 of 99.7% purity by the supplier, Sigma-Aldrich), rutile (α-TiO_2, 99.9+% purity, Sigma-Aldrich), and Min-U-Sil 5 natural quartz (α-SiO_2, ∼98.3% purity, U.S. Silica, Berkeley Springs, WV) were cleaned prior to use by dialysis in deionized (DI) water. All water used in these experiments was purified with a Barnstead Nanopure Diamond system (Barnstead, Dubuque, IA) to a resistivity of 18.2 MΩ.

2.2. Particle Characterization. Relevant physical and chemical characteristics are listed in Table 1. The purity of the oxide phases was verified by X-ray diffraction on a Scintag PADV X-ray diffractometer (Thermo Fisher Scientific, Waltham, MA) equipped with a Cu Kα tube and operated at 45 kV and 40 mA. The purity of the quartz and rutile samples was confirmed (Supporting Information, Figure 1a,b). The corundum sample was ∼80% pure, as determined using a standard addition method,[86] the primary impurity being very slightly cation-substituted aluminum oxide

(25) Reimhult, E.; Höök, F.; Kasemo, B. *Langmuir* **2003**, *19*, 1681−1691.
(26) Seantier, B.; Breffa, C.; Félix, O.; Decher, G. *J. Phys. Chem. B* **2005**, *109*, 21755−21765.
(27) Richter, R. P.; Brisson, A. R. *Biophys. J.* **2005**, *88*, 3422−3433.
(28) Keller, C. A.; Kasemo, B. *Biophys. J.* **1998**, *75*, 1397−1402.
(29) Gutberlet, T.; Steitz, R.; Fragneto, G.; Klösgen, B. *J. Phys.: Condens. Matter* **2004**, *16*, S2469−S2476.
(30) Efremov, A.; Mauro, J. C.; Raghavan, S. *Langmuir* **2004**, *20*, 5724−5731.
(31) Er, Y.; Prestidge, C. A.; Fornasiero, D. *Colloid Surf. B* **2004**, *36*, 147−153.
(32) Rädler, J.; Strey, H.; Sackmann, E. *Langmuir* **1995**, *11*, 4539−4548.
(33) Jass, J.; Tjärnhage, T.; Puu, G. *Biophys. J.* **2000**, *79*, 3153−3163.
(34) Egawa, H.; Furusawa, K. *Langmuir* **1999**, *15*, 1660−1666.
(35) Reviakine, I.; Brisson, A. *Langmuir* **2000**, *16*, 1806−1815.
(36) Dufrêne, Y. F.; Lee, G. U. *Biochim. Biophys. Acta* **2000**, *1509*, 14−41.
(37) Muresan, A. S.; Lee, K. Y. C. *J. Phys. Chem. B* **2001**, *105*, 852−855.
(38) Richter, R.; Mukhopadhyay, A.; Brisson, A. *Biophys. J.* **2003**, *85*, 3035−3047.
(39) Schönherr, H.; Johnson, J. M.; Lenz, P.; Frank, C. W.; Boxer, S. G. *Langmuir* **2004**, *20*, 11600−11606.
(40) Seantier, B.; Breffa, C.; Félix, O.; Decher, G. *Nano Lett.* **2004**, *4*, 5−10.
(41) McKiernan, A. E.; Ratto, T. V.; Longo, M. L. *Biophys. J.* **2000**, *79*, 2605−2615.
(42) Rossetti, F. F.; Bally, M.; Michel, R.; Textor, M.; Reviakine, I. *Langmuir* **2005**, *21*, 6443−6450.
(43) Keller, C. A.; Glasmästar, K.; Zhdanov, V. P.; Kasemo, B. *Phys. Rev. Lett.* **2000**, *84*, 5443−5446.
(44) Lüthgens, E.; Herrig, A.; Kastl, K.; Steinem, C.; Reiss, B.; Wegener, J.; Pignataro, B.; Janshoff, A. *Meas. Sci. Technol.* **2003**, *14*, 1865−1875.
(45) Bene, M.; Billy, D.; Benda, A.; Speijer, H.; Hof, M.; Hermens, W. T. *Langmuir* **2004**, *20*, 10129−10137.
(46) Nollert, P.; Kiefer, H.; Jähnig, F. *Biophys. J.* **1995**, *69*, 1447−1455.
(47) Cremer, P. S.; Boxer, S. G. *J. Phys. Chem. B* **1999**, *103*, 2554−2559.
(48) Johnson, J. M.; Ha, T.; Chu, S.; Boxer, S. G. *Biophys. J.* **2002**, *83*, 3371−3379.
(49) Gutberlet, T.; Klösgen, B.; Krastev, R.; Steitz, R. *Adv. Eng. Mater.* **2004**, *6*, 832−836.
(50) Vacklin, H. P.; Tiberg, F.; Fragneto, G.; Thomas, R. K. *Langmuir* **2005**, *21*, 2827−2837.
(51) Dimitrievski, K.; Reimhult, E.; Kasemo, B.; Zhdanov, V. P. *Colloid Surf. B* **2004**, *39*, 77−86.
(52) Seifert, U.; Lipowsky, R. *Phys. Rev. A* **1990**, *42*, 4768−4771.
(53) Lipowsky, R.; Seifert, U. *Langmuir* **1991**, *7*, 1867−1873.
(54) Reimhult, E.; Höök, F.; Kasemo, B. *J. Chem. Phys.* **2002**, *117*, 7401−7404.
(55) Käsbauer, M.; Junglas, M.; Bayerl, T. M. *Biophys. J.* **1999**, *76*, 2600−2605.
(56) Kim, J.; Kim, G.; Cremer, P. S. *Langmuir* **2001**, *17*, 7255−7260.
(57) Rapuano, R.; Carmona-Ribeiro, A. M. *J. Colloid Interface Sci.* **2000**, *226*, 299−307.
(58) Ekeroth, J.; Konradsson, P.; Höök, F. *Langmuir* **2002**, *18*, 7923−7929.
(59) Boudard, S.; Seantier, B.; Breffa, C.; Decher, G.; Félix, O. *Thin Solid Films* **2006**, *495*, 246−251.
(60) Moura, S. P.; Carmona-Ribeiro, A. M. *Langmuir* **2005**, *21*, 10160−10164.
(61) Reimhult, E.; Höök, F.; Kasemo, B. *Phys. Rev. E* **2002**, *66*, 051905.
(62) Chan, V.; Wan, K. T. *Langmuir* **2002**, *18*, 3134−3141.
(63) Wiegart, L.; Struth, B.; Tolan, M.; Terech, P. *Langmuir* **2005**, *21*, 7349−7357.
(64) Naumann, C.; Brumm, T.; Bayerl, T. M. *Biophys. J.* **1992**, *63*, 1314−1319.
(65) Lee, C. S.; Bain, C. D. *Biochim. Biophys. Acta* **2005**, *1711*, 59−71.
(66) Junglas, M.; Danner, B.; Bayerl, T. M. *Langmuir* **2003**, *19*, 1914−1917.
(67) Salamon, Z.; Tollin, G. *Biophys. J.* **2001**, *80*, 1557−1567.
(68) Hughes, A. V.; Roser, S. J.; Gerstenberg, M.; Goldar, A.; Stidder, B.; Feidenhans'l, R.; Bradshaw, J. *Langmuir* **2002**, *18*, 8161−8171.
(69) Liu, J.; Conboy, J. C. *Langmuir* **2005**, *21*, 9091−9097.
(70) Xie, A. F.; Yamada, R.; Gewirth, A. A.; Granick, S. *Phys. Rev. Lett.* **2002**, *89*, 246103.
(71) Tero, R.; Watanabe, H.; Urisu, T. *Phys. Chem. Chem. Phys.* **2006**, *8*, 3885−3894.
(72) Rossetti, F. F.; Textor, M.; Reviakine, I. *Langmuir* **2006**, *22*, 3467−3473.
(73) Richter, R. P.; Bérat, R.; Brisson, A. R. *Langmuir* **2006**, *22*, 3497−3505.
(74) Cha, T.; Guo, A.; Zhu, X. Y. *Biophys. J.* **2006**, *90*, 1270−1274.
(75) Richter, R. P.; Maury, N.; Brisson, A. R. *Langmuir* **2005**, *21*, 299−304.
(76) Wiegart, L.; O'Flaherty, S. M.; Struth, B. *Langmuir* **2005**, *21*, 1695−1698.
(77) Faiss, S.; Lüthgens, E.; Janshoff, A. *Eur. Biophys. J.* **2004**, *33*, 555−561.
(78) Zawisza, I.; Lachenwitzer, A.; Zamlynny, V.; Horswell, S. L.; Goddard, J. D.; Lipkowski, J. *Biophys. J.* **2003**, *85*, 4055−4075.
(79) Bin, X.; Zawisza, I.; Goddard, J. D.; Lipkowski, J. *Langmuir* **2005**, *21*, 330−347.
(80) Jenkins, A. T. A.; Bushby, R. J.; Evans, S. D.; Knoll, W.; Offenhäusser, A.; Ogier, S. D. *Langmuir* **2002**, *18*, 3176−3180.
(81) Stevens, M. J. Oxide-specific phospholipid adsorption and jurkat cell adhesion. M.S. Thesis, University of Wisconsin−Madison, Madison, WI, 2007.
(82) Scott, M. J.; Jones, M. N. *Colloid Surf. A* **2002**, *207*, 69−79.
(83) Jiang, C. H.; Gamarnik, A.; Tripp, C. P. *J. Phys. Chem. B* **2005**, *109*, 4539−4544.
(84) Reviakine, I.; Rossetti, F. F.; Morozov, A. N.; Textor, M. *J. Chem. Phys.* **2005**, *122*, 204711.
(85) Groves, J. T.; Ulman, N.; Cremer, P. S.; Boxer, S. G. *Langmuir* **1998**, *14*, 3347−3350.
(86) Jenkins, R.; Snyder, R. L. *Introduction to X-ray Powder Diffractometry*; John Wiley & Sons, Inc.: New York, 1996.

Table 1. Relevant Physical and Chemical Characteristics for the Oxide Particles Used in This Study

oxide	pH_{pzc}[a,b] (at 25 °C)	Hamaker constant[c,d] (10^{-20} J)	mean particle diameter[e] (nm)	polydispersity[e]	BET surface area ($m^2 \cdot g^{-1}$)
quartz (α-SiO_2)	2.9	1.76	1369 ± 146	0.256	6.04
rutile (α-TiO_2)	5.8	6.0	977 ± 26.2	0.231	3.26
corundum (α-Al_2O_3)	9.4	2.75	2500[f]	n/a	1.17

[a] Reference 98. [b] Reference 101. [c] Reference 107. [d] Reference 109. [e] *z*-Average diameters and polydispersities are means of at least seven measurements. [f] Manufacturer-provided (Sigma-Aldrich) value.

Table 2. Solution Conditions Used in This Study with Corresponding Diffuse Layer Thicknesses and Measured Vesicle Sizes[a]

solution conditions (mM)[b]							
pH	$[Na^+]$	$[Ca^{2+}]$	$[Cl^-]$	IS	$1/\kappa$ (nm)	average vesicle diameter[c] (nm)	polydispersity[c]
5.0	20	0	13	16.5	2.3	47.9	0.163
7.2	20	0	0	10	3.0	56.3	0.169
9.0	50	0	0	25	1.9	54.8	0.208
7.2	107	2	91	103	0.93	55.0	0.163

[a] All solutions were prepared in 50 mM HEPES buffered solution. [b] See the text for an explanation of ionic strength variations. [c] Vesicle *z*-average diameters and polydispersities are means of five measurements.

phases (e.g., $NaAl_{11}O_{17}$) (Supporting Information, Figure 1c). The mixture is considered here as pure corundum.

Average particle diameters (Table 1) were determined by dynamic light scattering (DLS) using a ZetaSizer Nano ZS instrument (Malvern Instruments, Worcestershire, UK), equipped with a 633 nm laser. Aqueous suspensions of the particles (0.05−0.5 mg mL^{-1}) were dispersed by brief sonication for ∼1 min prior to analysis, and a 60 nm latex size standard (Duke Scientific, Fremont, CA) was used prior to each experiment to ensure proper instrument performance. Reliable measurements could not be determined for the corundum sample due to rapid sedimentation of the particles, so the manufacturer-stated value (measured by Fisher subsieve) is indicated in Table 1.

Specific surface areas and porosities were analyzed using a Nova 4200e surface area and pore size analyzer (Quantachrome Instruments, Boynton Beach, FL). Specific surface areas were determined by multipoint Brunauer−Emmett−Teller (BET) N_2 gas adsorption isotherms between relative pressures (P/P_0) of 0.05 and 0.30.[87] Surface areas listed in Table 1 are mean averages of at least three separate measurements. Oxide porosity was determined by Barrett, Joyner, and Halenda (BJH) analysis of the N_2 desorption curve above a P/P_0 value of 0.35.[88] On the basis of low values for total pore volume (∼0.001−0.01 $mL \cdot g^{-1}$) and average pore diameter (∼3.2 nm), the porosity of the particles was considered negligible.

Particle morphologies were examined in vacuum with a Hitachi S-3400N scanning electron microscope (SEM) (Hitachi High Technologies America, Inc., Pleasanton, CA) using secondary electron emission. Individual particles of quartz, rutile, and corundum were observed of approximate sizes, in agreement with particle diameters obtained by DLS (Table 1). Quartz particles appeared predominantly angular in shape (Supporting Information, Figure 2a), whereas rutile particles had rounded edges and a tabular morphology (Supporting Information, Figure 2b). Corundum particles were a roughly equal mixture of round-edged tabular and angular shapes (Supporting Information, Figure 2c).

2.3. Vesicle Solution Preparation. All glassware used in these preparations was initially treated with Sigmacote (Sigma-Aldrich), which produces a neutral, hydrophobic film on glass, in order to minimize lipid loss by sorption to the hydrophilic glass surface. Buffer solutions were prepared to pH 7.2[89] and then adjusted as needed with either 0.5 M NaOH or 0.6 M HCl. Addition of these reagents accounts for the small differences in ionic strength indicated in Table 2. The high ionic strength solution was prepared by adding NaCl and $CaCl_2$ to the initial buffer solution. Necessary volumes of DPPC in chloroform were dispensed into a small glass vial. Solvent was removed under a light nitrogen flow and then under vacuum in a desiccating bowl. The dried DPPC film was hydrated with preheated (∼60 °C) buffer solution (0.05 M HEPES) to give a final lipid concentration of 1−1.5 mM, thermostated at ∼60 °C (i.e., above the gel−liquid crystal phase transition temperature) for 2 h in a water bath (Fisher Isotemp 205), and stored at 0 °C.

Prior to use, solutions were again thermostated at ∼60 °C and bath-sonicated (Branson 3510, Branson Ultrasonics, Danbury, CT) to produce small unilamellar vesicles (SUV) until maximum solution clarity was achieved (typically 1−2 h). Finally, vesicle solutions were centrifuged (Avanti J-E centrifuge, Beckman Coulter, Inc., Fullerton, CA) for 1 h at 53 000*g* and 22 °C in order to remove multilamellar structures, which have been shown to influence adsorption results.[90] The supernatant was removed with a micropipette for use. The average size of vesicles prepared with this procedure was measured by DLS as described above (Table 2).

2.4. Determination of Lipid Concentration. DPPC concentrations were determined using a variation of a common colorimetric method for inorganic phosphorus (P_i) analysis.[91] Triplicate aliquots of the solutions before and after reaction in oxide suspension were analyzed. Each 50 μL aliquot was heated for 1.75 h at 185 °C with 300 μL of perchloric acid in order to digest the phospholipid. After cooling, 1 mL of water and 400 μL each of 0.01 M ammonium molybdate tetrahydrate and 0.28 M ascorbic acid solutions were added, forming a reduced phospho−molybdate complex. Sample solutions were thoroughly mixed after each addition and were then heated at 100 °C for 8 min to develop color. Absorbance was measured by UV−vis spectrophotometry at 797 nm (UV-Mini 1240 UV−vis spectrophotometer, Shimadzu Corp., Kyoto, Japan).

2.5. Adsorption Isotherms. Isotherms were obtained at 55 °C, above the main L_β (gel) to L_α (liquid-crystal) phase transition temperature of DPPC (41 °C),[92,93] because the less ordered liquid-crystal phase is physiologically more relevant.[94]

Oxide suspensions were prepared by adding 750 μL of 0.05 M HEPES solution into 1.5 mL microcentrifuge tubes containing known masses of oxide, followed by vortexing and sonicating to disperse the particles. DPPC vesicle solutions of varying concentration were

(87) Brunauer, S.; Emmett, P. H.; Teller, E. *J. Am. Chem. Soc.* **1938**, *60*, 309−319.
(88) Barrett, E. P.; Joyner, L. G.; Halenda, P. P. *J. Am. Chem. Soc.* **1951**, *73*, 373−380.
(89) Dawson, R. M. C.; Elliott, D. C.; Elliott, W. H.; Jones, K. M. *Data for Biochemical Research*, 3rd ed.; Oxford University Press: Oxford, 1986.
(90) Rapuano, R.; Carmona-Ribeiro, A. M. *J. Colloid Interface Sci.* **1997**, *193*, 104−111.
(91) Rouser, G.; Fleischer, S.; Yamamoto, A. *Lipids* **1970**, *5*, 494-496.
(92) Marsh, D. *CRC Handbook of Lipid Bilayers*; CRC Press: Boca Raton, FL, 1990.
(93) Liu, H. C.; Turcotte, J. G.; Notter, R. H. *Langmuir* **1995**, *11*, 101−107.
(94) Nagle, J. F.; Tristram-Nagle, S. *Biochim. Biophys. Acta* **2000**, *1469*, 159−195.

diluted from a stock solution. After preparation, an equal volume (250 μL) of each concentration was added to two microcentrifuge tubes containing either 750 μL of an oxide suspension or 750 μL of 0.05 M HEPES buffer solution alone. The tubes were then capped and vortexed again for about 10 s in order to ensure thorough mixing. The microcentrifuge tubes were thermostated overnight (>12 h) at 55 °C in a water bath (equilibrium is achieved in ~1 h[57,90]) and then centrifuged for 80 min at 28 000*g* and 22 °C. Aliquots (50 μL) of supernatant solutions were sampled using a 10−50 μL micropipette. Tubes containing DPPC + buffer were analyzed for total initial DPPC concentration ($[DPPC]_{aq,i}$), while tubes containing oxide + DPPC + buffer were analyzed for final concentration ($[DPPC]_{aq,f}$). Adsorbed DPPC was taken as the difference in DPPC concentration between the initial solution concentration ($[DPPC]_{aq,i}$) and the final, or equilibrium, concentration in the supernatant ($[DPPC]_{aq,f} = [DPPC]_{eq}$). This value was normalized to the available oxide surface area to obtain isotherms in terms of DPPC adsorbed in μmol m^{-2} versus the equilibrium DPPC concentration ($[DPPC]_{eq}$) in solution in mM units.

In the following adsorption isotherm figures, lines drawn through the data are box-averaged interpolation fits (where the adsorption value at a given point is averaged with the two preceding and two following points) to guide the reader's eye. Error bars indicate one standard deviation based on triplicate analysis. The adsorbed concentrations and standard deviations are normalized to the total available oxide surface area. Thus, the error estimates are inversely proportional to the total surface area, resulting in larger apparent errors and scatter of data for oxides with smaller specific surface areas. The error bars also generally trend toward larger magnitudes with increasing DPPC concentration in solution. This effect is likely due to greater inconsistency in the delivery of pipetted aliquots at higher concentrations, where the lipid solutions have a higher viscosity.

3. Results

3.1. Effect of Oxides. Adsorption of DPPC on the three oxides at each pH is compared in Figure 1. On quartz at all pH values and on rutile at pH 7.2 and 9, adsorption increases initially with increasing solution concentration and then levels off at a DPPC concentration of ~0.3−0.5 mM in solution. In contrast, adsorption on corundum at all pHs and on rutile at pH 5 shows a further increase beyond the initial plateau. At pH 5.0, we observe a plateau coverage of ~20−22 μmol m^{-2} for corundum and rutile but only ~13 μmol m^{-2} on negatively charged quartz (Figure 1a). A substantially higher adsorption plateau of 20−25 μmol m^{-2} is obtained on corundum at pH 7.2 compared to rutile and quartz, both at ~13 μmol m^{-2} (Figure 1b). The same trend is seen at pH 9.0, where the maximum adsorption on corundum, ~20 μmol m^{-2}, is still the greatest among the oxides (Figure 1c), though slightly decreased relative to its value at pH 7.2, and rutile and quartz again have similar adsorption plateaus at ~10−11 μmol m^2.

3.2. Effect of pH. The same adsorption data are replotted in Figure 2 to highlight the effect of pH on each oxide. The adsorption isotherms at pH 5.0 and 7.2 for quartz overlap considerably, while less adsorption is seen at pH 9.0 (Figure 2a). The isotherms for rutile at pH 5.0, 7.2, and 9.0 (Figure 2b) are clearly distinguished over most of the range of DPPC concentrations studied, indicating plateau coverages, respectively, of ~20, 13, and 10 μmol m^{-2}. For corundum, the isotherms at pH 5.0 and 7.2 overlap considerably (Figure 2c), and adsorption is only slightly lower at pH 9.0.

Significantly, the maximum adsorption on positively charged oxide surfaces is approximately 1.5−2 times greater than on negatively charged surfaces. Considering an area per headgroup of 0.64 nm^2 for liquid crystalline DPPC,[94] an adsorption total of ~5.2 μmol m^{-2} corresponds to full bilayer coverage on the oxides. Thus, plateau adsorption values observed on negative surfaces approximately indicate coverage by two stacked bilayers, while greater values on positive surfaces indicate four or more stacked bilayers. In summary, both the amount indicated by and the shape of the DPPC adsorption isotherms depend on the type of oxide and on pH.

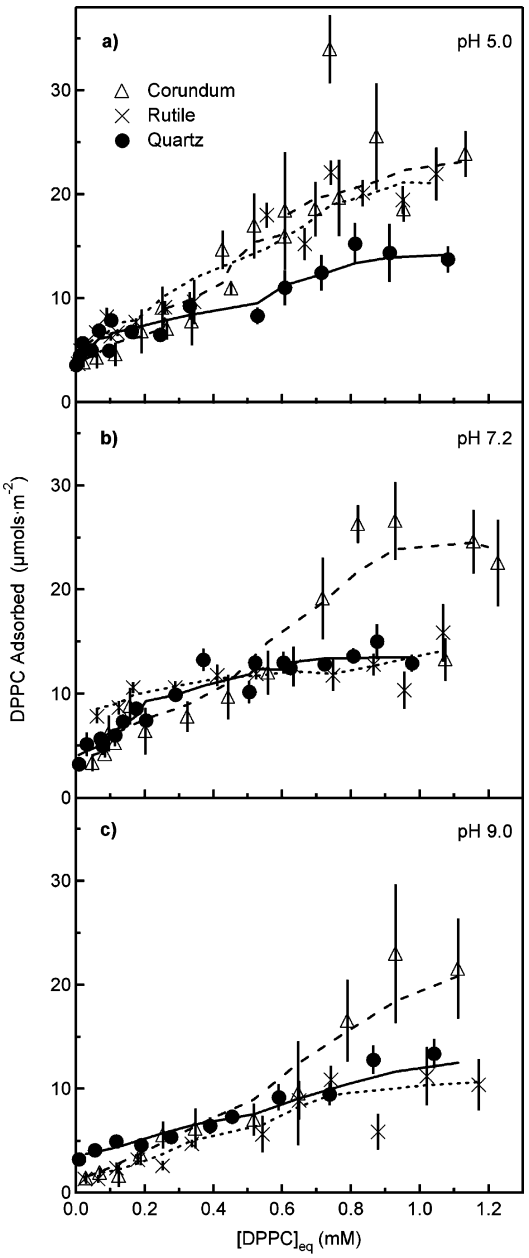

Figure 1. Equilibrium adsorption of DPPC from bulk solution at pH 5.0, 7.2, and 9.0 onto quartz, rutile, and corundum particles at 55 °C in 50 mM HEPES (see Table 2 for ionic strength conditions). Error bars represent one standard deviation based on spectrophotometric analysis of triplicate solution samples. Box-averaged fit lines (dashed, pH 5.0; dotted, pH 7.2; solid, pH 9.0) are shown to guide the eye.

3.3. Effect of Ionic Strength and Ca^{2+}. Adsorption isotherms were obtained at pH 7.2 under different ionic strength and electrolyte cation conditions, ~100 mM Na^+ with 2 mM Ca^{2+} (Figure 3, Table 2). The conditions were chosen to mimic physiological concentrations of Na^+ and Ca^{2+} [95] and to vary Na^+ concentration by an order of magnitude. Comparing Figure 3 to

(95) Kokubo, T.; Takadama, H. *Biomaterials* **2006**, *27*, 2907−2915.

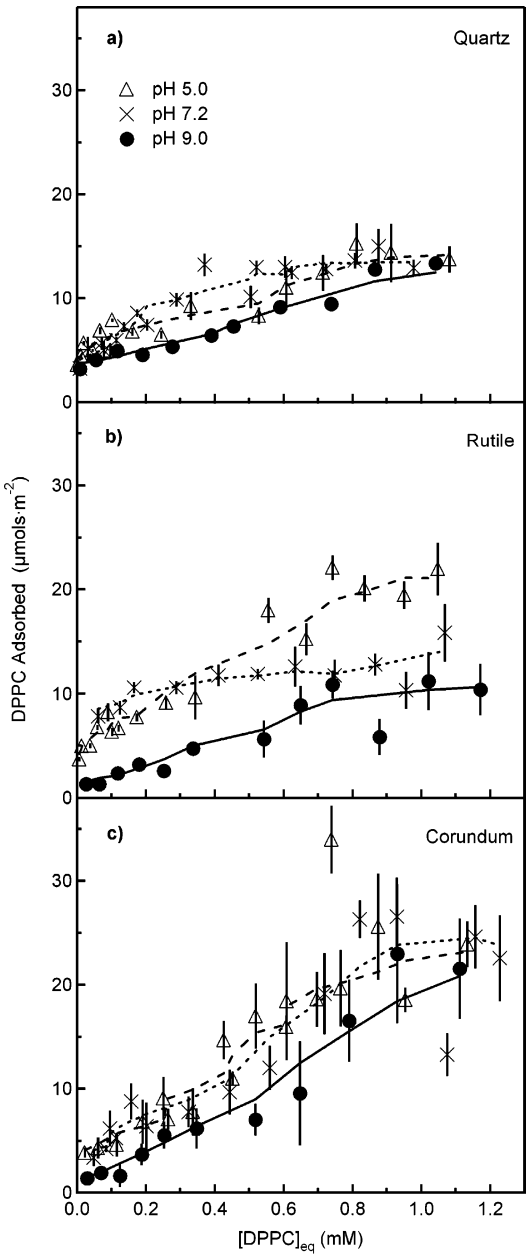

Figure 2. Equilibrium adsorption of DPPC from bulk solution onto quartz, rutile, and corundum particles at 55 °C for pH 5.0, 7.2, and 9.0 in 50 mM HEPES (see Table 2 for ionic strength conditions). Error bars represent one standard deviation based on spectrophotometric analysis of triplicate solution samples. Box-averaged fit lines (dashed, corundum; dotted, rutile; solid, quartz) are shown to guide the eye.

the corresponding plot at lower ionic strength (Figure 1b), we see that the general adsorption trend of corundum > rutile ≈ quartz is maintained. Adsorption on each oxide is similar at both ionic strengths up to a concentration of ∼0.5 mM free DPPC. Above this concentration, the isotherms level off at coverages of 20−25 μmol m^{-2} for corundum and ∼13 μmol m^{-2} for rutile and quartz at the lower ionic strength. At the higher ionic strength, however, DPPC adsorption continues to rise and no plateau coverage is observed in the concentration range studied. The maximum coverages we observe are ∼30 μmol m^{-2} for corundum and ∼20 μmol m^{-2} for rutile and quartz at [DPPC]$_{eq}$ ≈ 1.1 mM (Figure 3). These values correspond, respectively, to roughly six and four bilayers, if the area per lipid headgroup is 0.64 nm^2.

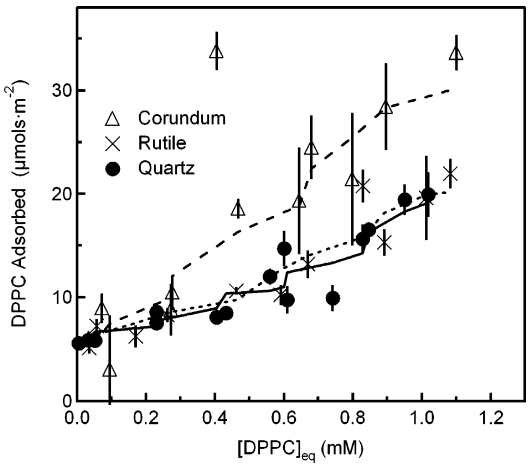

Figure 3. Equilibrium adsorption of DPPC from bulk solution onto quartz, rutile, and corundum particles at 55 °C at pH 7.2 in 50 mM HEPES with 107 mM Na^+ and 2 mM Ca^{2+}. Error bars represent one standard deviation based on spectrophotometric analysis of triplicate solution samples. Box-averaged fit lines (dashed, corundum; dotted, rutile; solid, quartz) are shown to guide the eye.

4. Discussion

4.1. Amphoteric Oxide Surfaces and Electrostatic Forces. Oxides have amphoteric hydroxyl surface sites that can take up or release protons, resulting in net positive, neutral, or negative surface charge. The protonation and deprotonation reactions of surface hydroxyls can be described by equilibrium reactions and their corresponding equilibrium acidity constants.[96,97] Each oxide has a characteristic pH known as the point of zero charge, where net surface charge is neutral and is related to the sum of the surface acidity constants.[96,97] Oxide surfaces are positively charged at pH < PZC and negatively charged at pH > PZC. The magnitude of surface charge at a given number of pH units away from the PZC is described by another characteristic property of the oxide, that is, the difference in the surface acidity constants (ΔpK_a). A large value of ΔpK_a generally indicates a small change in the magnitude of surface charge with pH change below or above the PZC.[98]

Quartz, rutile, and corundum have PZCs of, respectively, ∼3, 5.8, and 9.4 at 25 °C. At 55 °C, the PZCs are about half a log unit lower.[99,100] Thus, quartz is negatively charged and corundum is positively charged or near neutral over the entire pH range studied here, in contrast to rutile, whose PZC is encompassed by the experimental pH range. The results in Figures 1 and 2 can now be interpreted in terms of electrostatic attraction between the charged surface sites on the oxides and the headgroup of DPPC.

At pH 5.0, the greater DPPC uptake on both corundum and rutile is consistent with their positive surface charge, while quartz is negatively charged and, consequently, has lower uptake (Figure 1a). This trend suggests that the negatively charged phosphate ester (−R(PO$_4^-$)R′−) moiety of the headgroup is electrostatically attracted to the positively charged sites on corundum and rutile and is repelled by the negative charge on quartz. At pH 7.2,

(96) Sverjensky, D. A.; Sahai, N. *Geochim. Cosmochim. Acta* **1996**, *60*, 3773−3797.
(97) Schindler, P. W.; Stumm, W. In *Aquatic Surface Chemistry: Chemical Processes at the Particle-Water Interface*; Stumm, W., Ed.; John Wiley & Sons, Inc.: New York, 1987; pp 83−110.
(98) Sahai, N. *Environ. Sci. Technol.* **2002**, *36*, 445−452.
(99) Sverjensky, D. A.; Sahai, N. *Geochim. Cosmochim. Acta* **1998**, *62*, 3703−3716.
(100) Bérubé, Y. G.; De Bruyn, P. L. *J. Colloid Interface Sci.* **1968**, *27*, 305−323.

corundum is the only positively charged surface, whereas rutile and quartz have negative surface charges of similar magnitude,[101] consistent with the observation that uptake on rutile and quartz are similar and less than on corundum (Figure 1b). Finally, the charge on corundum is slightly positive to near neutral at pH 9.0, while quartz and rutile again have similar magnitudes of negative surface charge.[101] Uptake is still greater on corundum than on quartz and rutile at this high pH (Figure 1c), although the isotherms are noticeably depressed over the whole concentration range studied relative to their positions at lower pH.

The increase in negative charge on quartz is small from pH 5.0 to 7.2 because quartz has a large $\Delta pK_a = 8.4$,[96,98,101] explaining the similar amounts of uptake at pH 5.0 and 7.2 (Figure 2a). By pH 9.0, however, the magnitude of negative surface charge is sufficiently different so as to affect the adsorption of DPPC.[101] The surface of rutile is positively charged at pH 5.0, but becomes increasingly negative above its PZC (~5.8).[101] This change in surface charge is reflected in the isotherms, with maximum adsorption decreasing with increasing pH (Figure 2b).

The corundum surface has a positive charge over the pH range studied, but it is close to neutral at pH 9, consistent with lower adsorption. Corundum also has the most steeply increasing charge with pH away from its PZC (i.e., small $\Delta pK_a \sim 6$) such that the surface charge at pH 7.2 is only about half that at pH 5.0.[101] The overlap in the isotherms at pH 5.0 and 7.2 (Figure 2c) may thus indicate a limit on the electrostatic attraction between the positively charged corundum surface and the phosphate moiety of the DPPC headgroup. Alternatively, the isotherms at these pHs may simply represent saturation coverage of the available corundum surface, in which case the effect of additional positive surface charge at pH 5.0 would be obscured.

At 100 mM NaCl ionic strength, the higher ion concentration provides greater charge screening such that more surface charge may develop.[102] As seen above, there is a significant electrostatic attraction between the phosphate portion of the DPPC headgroup and positively charged oxide surface sites. For corundum, increasing the positive surface charge by raising the ionic strength may amplify electrostatic attraction with DPPC, thus leading to the increased adsorption. However, the fact that the quartz and rutile isotherms both show increased adsorption at high ionic strength, despite increased negative surface charge, and the limiting effect for adsorption on corundum (Figure 2c) argue against charge screening by monovalent ions as the sole cause for increased adsorption. A more likely explanation is based on the role of Ca^{2+}. Previous studies have indicated the ability of Ca^{2+} even at low (e.g., 1 mM) concentration to promote vesicle adsorption and bilayer formation on solid substrates.[26,27,33,35,38,45,58] Furthermore, divalent cations are known to bind strongly to the DPPC headgroup,[103] thereby screening repulsion, and perhaps promoting deposition of additional bilayer(s).

4.2. Nature of Electrostatic Interactions. From pH 5.0 to 9.0, adsorption decreases with increasing negative surface charge or decreasing positive charge. This observation suggests negligible electrostatic interactions, either attractive or repulsive, between negatively charged oxide surface sites and the positively charged alkylammonium moiety ($-RN(CH_3)_3^+$) in the DPPC headgroup. This is attributed to a lower positive charge density associated with the relatively bulky choline group compared to the negative charge density associated with the smaller phosphate ester moiety. Thus, the data suggest that the phosphate ester moiety of the headgroup is dominantly responsible for the electrostatic interaction between DPPC and charged surface sites, consistent with ^{1}H NMR data.[104]

4.3. Other Contributing Forces to DPPC Adsorption. Adsorption was observed over the whole pH range studied, even when the oxide surfaces are near neutral or negatively charged. Thus, electrostatic attraction alone cannot explain DPPC adsorption on the oxides. Furthermore, based solely on the electrostatic interaction, we would expect greater adsorption on corundum than on rutile at pH 5.0 because of the greater positive charge density on corundum.[101] In contrast to this expectation, however, adsorption on corundum and rutile is roughly equivalent at pH 5.0 (Figure 1a). These apparent anomalies to predictions based on electrostatic interactions suggest the role of additional force(s) driving DPPC adsorption on oxides.

The DPPC vesicles have a ~50 nm diameter, which is in the colloidal size range, so interactions with the oxides may be described in terms of Derjaguin−Landau−Verwey−Overbeek (DLVO) theory.[47,105] According to DLVO theory, interaction between colloidal particles is controlled by van der Waals and electrostatic forces. Non-DLVO forces such as hydration and steric forces may also be involved.[105,106] The hydration force acting between the oxide and the exposed DPPC headgroups is repulsive, as it is between any two hydrophilic particles in water.[106] In addition, so-called "steric" forces related to membrane undulation or bulging are proposed to arise from short-range intermolecular forces among lipid molecules, but act repulsively on a longer lateral scale.[103,105] Van der Waals interactions are the only consistently attractive force in our systems. Thus, van der Waals forces account for DPPC adsorption on the oxides, and adsorption is further modified by electrostatic interactions. The magnitude of the van der Waals attraction varies depending on the oxide (assuming the contribution of DPPC is essentially constant in each case).

While a detailed determination of the van der Waals forces in our experimental systems is beyond the scope of the current work, the magnitudes should scale with the Hamaker constant for two particles of each oxide interacting in an aqueous medium.[105,107] Reported values for oxide Hamaker constants vary depending on the method used to determine them, but they consistently trend as quartz < corundum < rutile (see Table 1 for representative values).[107−111] This trend suggests a greater van der Waals contribution for rutile than for corundum, so that overall adsorption on rutile and corundum is comparable at pH 5.0, even though rutile has a lower surface charge density than corundum (i.e., smaller electrostatic force contribution).

The effect of van der Waals forces on adsorption can be estimated by observing adsorption at or near an oxide's PZC, where the net neutral charge of the surfaces will minimize electrostatic interactions. Thus, the isotherm on corundum at pH 9.0, and the quartz isotherm at pH 5.0 (though two pH units greater than the PZC, quartz still has very

(101) Sahai, N.; Sverjensky, D. A. *Geochim. Cosmochim. Acta* **1997**, *61*, 2801−2826.
(102) Fuerstenau, D. W.; Pradip *Adv. Colloid Interface Sci.* **2005**, *114*, 9−26.
(103) Marra, J.; Israelachvili, J. *Biochemistry* **1985**, *24*, 4608−4618.
(104) Yuan, C.; Zhao, D.; Liu, A.; Jiazuan, N. *J. Colloid Interface Sci.* **1995**, *172*, 536−538.
(105) Israelachvili, J. *Intermolecular and Surface Forces*, 2nd ed.; Academic Press: London, 1992.
(106) van Oss, C. J. *Interfacial Forces in Aqueuos Media*, 2nd ed.; CRC Press: Boca Raton, FL, 2006.
(107) Ackler, H. D.; French, R. H.; Chiang, Y.-M. *J. Colloid Interface Sci.* **1996**, *179*, 460−469.
(108) Bergström, L. *Adv. Colloid Interface Sci.* **1997**, *70*, 125−169.
(109) Tan, G. L.; Lemon, M. F.; Jones, D. J.; French, R. H. *Phys. Rev. B* **2005**, *72*, 205117.
(110) Leong, Y.-K.; Ong, B.-C. *J. Chem. Eng. Jpn.* **2004**, *37*, 187−193.
(111) Fernández-Varea, J. M.; Garcia-Molina, R. *J. Colloid Interface Sci.* **2000**, *231*, 394−397.

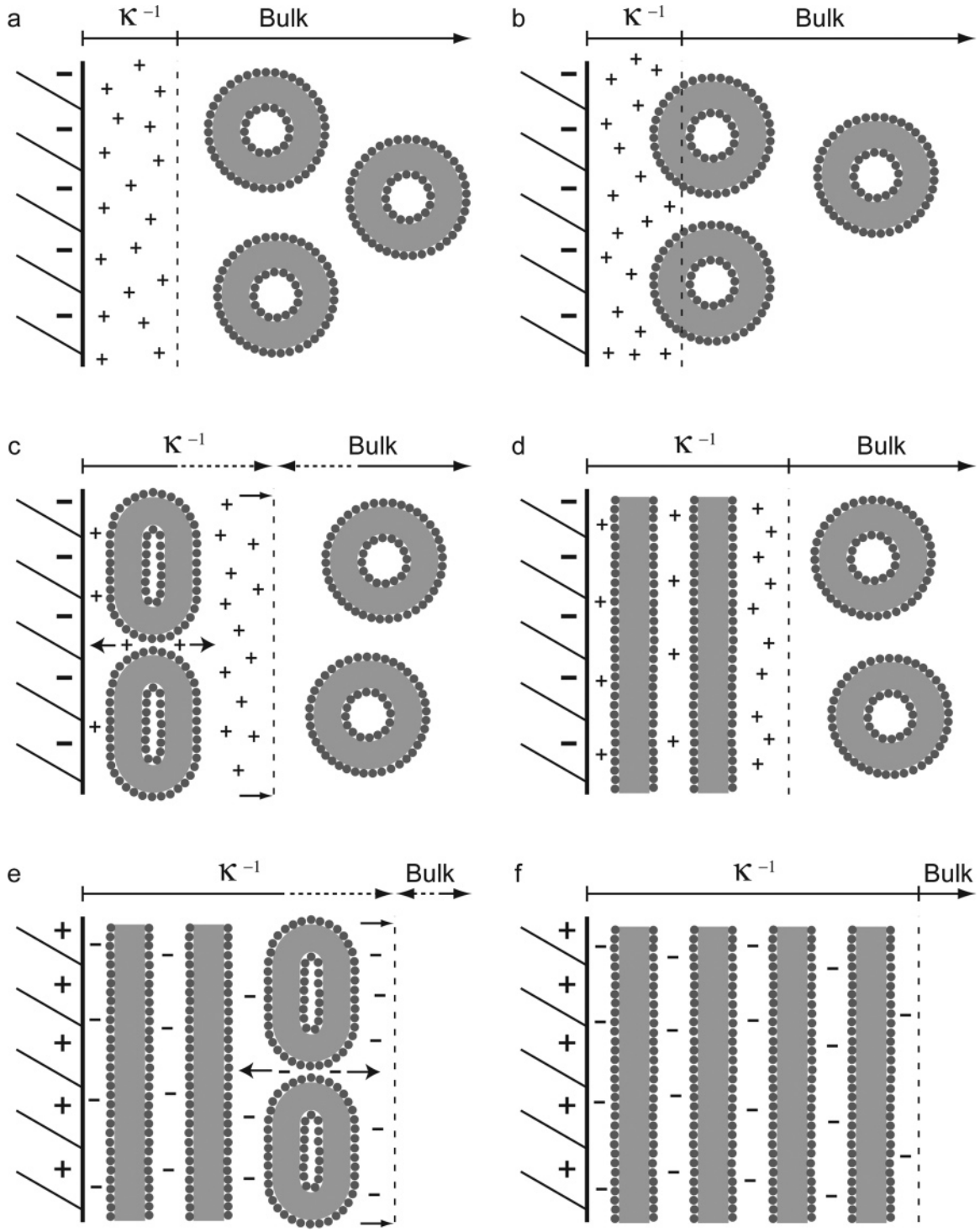

Figure 4. Proposed mechanism for adsorption of zwitterionic DPPC vesicles, followed by formation of supported bilayers, on charged oxide surfaces. Illustrations a−d apply for both negatively charged surfaces with positive counterions (as shown; e.g., quartz at pH 7.2) and positively charged surfaces with negative counterions (not shown; e.g., corundum at pH 5.0), while illustrations e and f apply only for the latter. Dashed lines indicate the boundary between the diffuse electric double layer, of thickness κ^{-1}, and bulk solution. (a) DPPC vesicles in bulk solution. (b) Initial adsorption driven by van der Waals forces. (c and d) Spreading, fusion, and rupture of vesicles to form a first and second SPB, with displacement of counterions from the near-surface region, effectively thickening the diffuse layer. (e and f) Adsorption of additional supported DPPC to form additional bilayers in the case of a positively charged oxide surface. Illustrations are not to scale.

low surface charge at this pH because its ΔpK_a is large), may be taken as the minimum, or "baseline", amount of adsorption on each oxide driven by van der Waals forces. Oxide- and pH-dependent electrostatic forces then modulate adsorption above or below this baseline level. Similar interactions were suggested to explain phosphatidylcholine adsorption on a glass substrate.[47]

4.4. The Oxide−DPPC Interface. Adsorption in the low concentration range (below ∼0.5 mM DPPC) is similar on all oxides. Only above this threshold concentration does adsorption increase markedly on the positive surfaces. As seen before, the phosphate moiety of the DPPC headgroup is the major contributor to the electrostatic interaction with the oxides. We expect, therefore, to see a difference in adsorption that depends on the

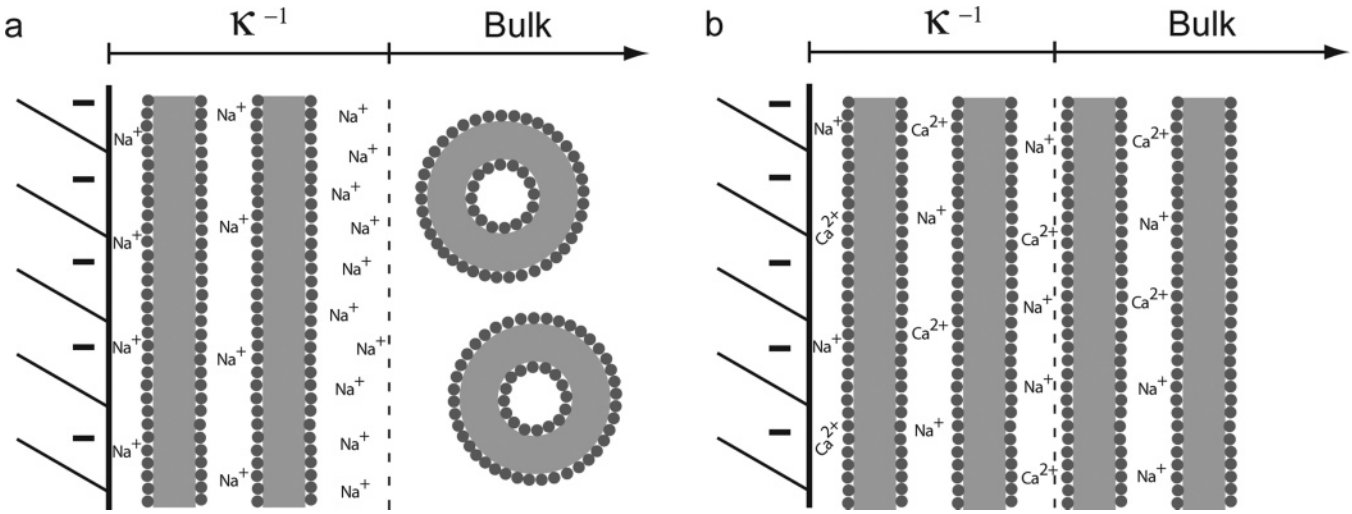

Figure 5. Greater DPPC adsorption is observed on our oxides, regardless of surface charge, under the higher ionic strength conditions (∼100 mM Na^+ with 2 mM Ca^{2+}) of our experiments. This likely results from decreased charge repulsion between headgroups in adjacent bilayers due to Ca^{2+} binding. (a) Formation of initial SPBs, similar to that shown in Figure 4d, when only a monovalent salt (Na^+) is present in solution. (b) In the presence of Ca^{2+}, additional adsorption beyond a single bilayer occurs. The additional DPPC may adsorb outside the diffuse layer of charge (denoted by a dashed line). Illustrations are not to scale.

sign of the oxide surface charge. Indeed, the maximum adsorption on positively charged surfaces (e.g., corundum and rutile at pH 5.0) is ∼20−25 μmol m^{-2}, roughly double the adsorption (∼10−13 μmol m^{-2}) achieved on negatively charged surfaces. This difference suggests the formation of additional DPPC bilayers on the former and is consistent with results obtained by atomic force microscopy showing increased bilayer stacking on a positively charged corundum surface, but not on several negatively charged oxide and mica surfaces (Supporting Information, Figure 3).[81] The formation of a different number of bilayers on negatively charged oxide surfaces versus positively charged surfaces has implications for the structure of the oxide−DPPC interface.

We do not have direct measurements of the electric−double layer structure of the oxide−DPPC interface, but our complete suite of oxides at different pHs, ionic strengths, and electrolyte ion types (Na^+ and Ca^{2+}) allows us to make some inferences. Prior NMR spectroscopy, neutron and X-ray reflectivity, and sum frequency generation studies have demonstrated the presence of an interfacial water layer of ∼0.4−1.5 nm thickness between solid substrates and phospholipid bilayers, offering evidence for the role of a repulsive hydration force.[29,47,56,112−114] The thickness of the intermediate water layer precludes the formation of direct covalent bonds or H-bonds between DPPC headgroups and oxide surface sites, which would require closer proximity of the two.

The evidence from our work points clearly to electrostatic interactions between the phosphate portion of the headgroup and oxide surface sites in addition to van der Waals interactions. These results suggest that the DPPC molecules must lie within the diffuse layer. DPPC is a zwitterion and has a net neutral charge, however, so it cannot act as a counterion though it may lie in the diffuse layer. The countercharge must be provided by other ions (e.g., Na^+ or Cl^-). If the DPPC molecules lie within the diffuse layer, one must compare the thickness of the diffuse layer with that of the DPPC bilayer(s).

We can estimate the thickness of the diffuse layer around a bare oxide particle by determining the Debye length ($1/\kappa$) from the expression[115]

$$\kappa^2 = (e^2/\epsilon_0 \epsilon kT)\sum_i n_i z_i^2 \quad (1)$$

where e is the charge on an electron, ϵ_0 is the permittivity of free space, ϵ is the dielectric constant of the medium, k is the Boltzmann constant, T is absolute temperature, n_i is the concentration (in number density), and z_i is the charge of the ith ionic species. Using the solution compositions at each pH (Table 2) and ϵ_{water} = 68.3 at 55 °C,[116] we calculate values of $1/\kappa$ ranging from ∼0.9 to 3.0 nm (Table 2).

By comparison, each DPPC bilayer is ∼5 nm thick.[94] The maximum coverages obtained in the isotherms indicate that at least two bilayers are formed on all oxide surfaces. These results suggest a restructuring of the diffuse layer around oxides in the presence of DPPC.

Based on the above observations, we propose the following model for DPPC adsorption on oxides (Figure 4). Initially, DPPC vesicles reside in the bulk solution phase (Figure 4a). Oxide surface charge is balanced by counterions (e.g., Na^+ or Cl^-) in the diffuse layer of initial thickness $\kappa^{-1} \approx 0.9-3.0$ nm. Brownian motion brings vesicles close enough to the surface such that they adsorb primarily due to attractive van der Waals forces (Figure 4b). The vesicles deform (Figure 4c), fuse, and rupture to form a first bilayer, corresponding to ∼5.2 μmol m^{-2} coverage. Cryoelectron microscopy images show a complete bilayer formed on colloidal silica particles at low $[PL]_{eq}$ (∼0.06 mM),[113] in agreement with our adsorption data at similar DPPC concentrations. The bilayer displaces counterions, and because bilayers are impermeable to counterions, the diffuse layer around the oxide particles is extended or thickened (Figure 4c). The diffuse layer is further extended through formation of a second bilayer, indicated by ∼10−11 μmol m^{-2} adsorption, on each of the oxides (Figure 4d). Using values of 0.5−1.5 nm for the oxide−DPPC interfacial water layer, ∼5 nm for the DPPC bilayer, and ∼2−3 nm for another water layer[117] between the first and second DPPC

(112) Miller, C. E.; Majewski, J.; Kuhl, T. L. *Colloid Surf. A* **2006**, *284*, 434−439.
(113) Mornet, S.; Lambert, O.; Duguet, E.; Brisson, A. *Nano Lett.* **2005**, *5*, 281−285.
(114) White, R. J.; Zhang, B.; Daniel, S.; Tang, J. M.; Ervin, E. N.; Cremer, P. S.; White, H. S. *Langmuir* **2006**, *22*, 10777−10783.
(115) Adamson, A. W.; Gast, A. P. *Physical Chemistry of Surfaces*, 6th ed.; John Wiley & Sons, Inc.: New York, 1997.
(116) *CRC Handbook of Chemistry and Physics*, student ed.; Lide, D. R., Ed.; CRC Press, Inc.: Boca Raton, FL, 1996.
(117) Charitat, T.; Bellet-Amalric, E.; Fragneto, G.; Graner, F. *Eur. Phys. J. B* **1999**, *8*, 583−593.

bilayers, we estimate a distance of ~7.5−9.5 nm from the oxide surface to the inner leaflet of the second DPPC bilayer. Van der Waals forces are diminished at this distance from the oxide surface, but they still operate, resulting in formation of the second bilayer.[105] The diminished strength of the van der Waals forces at these distances may also explain the decreased slope of the isotherms at coverages greater than ~5.2 μmol m^{-2}.

The difference between negatively and positively charged surfaces becomes evident at this stage. Adsorption is effectively halted at this point on negatively charged surfaces, because the van der Waals attraction is too weak beyond the second bilayer (~14.5−17.5 nm) and the dominant electrostatic interaction is repulsive. For a positively charged oxide surface, however, the electric field in the extended diffuse layer attracts the negatively charged ($-R(PO_4^-)R'-$) moiety in the headgroups of nearby vesicles (Figure 4e). From our data, at least two additional bilayers may adsorb (Figure 4f), although the morphology (e.g., full bilayer, adsorbed vesicles) of the outermost layer cannot be determined.

Finally, the role of Ca^{2+} accounts for adsorption beyond the second bilayer on all oxides at pH 7.2, including those with negatively charged surfaces. Under conditions where only a monovalent ion like Na^+ is present, only two SPBs form (Figure 5a). However, divalent Ca^{2+} binds strongly to, and screens electrostatic repulsion among, DPPC headgroups,[103] allowing deposition of additional bilayer(s) (Figure 5b). The additional DPPC may adsorb outside the diffuse layer, implying that there is no electrostatic interaction with the oxide surface.

A couple additional points should be noted regarding the model presented. First, total adsorption varies somewhat depending on the van der Waals interaction between DPPC and each oxide as well as on the oxide surface charge *density*, not simply the sign of the charge. As a result, subtle differences arise between similarly charged oxides in the isotherms. Second, we have assumed full bilayer coverage based on the adsorption values in our isotherms. Past work with AFM and other techniques has shown that formation of full, defect-free bilayers is subject to a variety of factors (e.g., substrate surface morphology) not specifically considered here.[73]

5. Conclusions

DPPC adsorption depends on the sign and density of oxide surface charge, which are determined by the oxide's PZC and ΔpK_a properties. Adsorption is driven primarily by van der Waals forces with contributions from electrostatic interactions between the phosphate ester ($-R(PO_4^-)R'-$) moiety of the DPPC headgroup and charged surface sites. In the presence of monovalent background electrolyte ions, two stacked SPBs will adsorb on either negative or positive oxide surfaces due to attractive van der Waals forces. Surface charge-neutralizing counterions are displaced during formation of the SPBs, extending the diffuse layer and allowing DPPC to interact electrostatically with charged surface sites over a longer distance. This results in formation of additional bilayer(s) on positively charged oxides, while negative surfaces repel additional vesicles, limiting adsorption to the initial two bilayers. Addition of divalent Ca^{2+} promotes adsorption beyond the second SPB, regardless of oxide surface charge.

Acknowledgment. The authors acknowledge Prof. Anant Menon (Cornell University Weill Medical College, New York) and his former postdoctoral researcher, Dr. Henna Ohvo-Rekila, for introducing us to the phosphorus analysis technique; Prof. Eric Roden (University of Wisconsin—Madison) for the use of the UV−vis spectrophotometer; and Prof. Huifang Xu, Prof. Joel Pedersen, Dr. John Fournelle, Dr. Walt Zeltner, Dr. Xin Ma, and Rakesh Reddy (University of Wisconsin—Madison) for assistance with particle characterization. We thank U.S. Silica for generously donating the Min-U-Sil 5 quartz. We are grateful to the two anonymous reviewers for their constructive comments regarding our manuscript. This work was funded by the following grants to N.S.: NSF Career Award (EAR 0346889), American Chemical Society Petroleum Research Fund (41777-AC2), Wisconsin Alumni Research Foundation (WARF) Award, and "faculty start-up" funds from the University of Wisconsin-Madison and the Department of Geology and Geophysics; T.A.O. was also partially supported by a Geological Society of America Graduate Research grant.

Supporting Information Available: Results from XRD and SEM analyses of the quartz, rutile, and corundum particles used in this study are provided, as well as atomic force microscope images of DPPC on several planar substrates. This material is available free of charge via the Internet at http://pubs.acs.org.

LA703599G